analytical chemistry

Article

Chromogenic, fluorescent and redox sensors for multichannel imaging and detection of hydrogen peroxide in living cell systems

Yue Ni, Hong Liu, Di Dai, Xiqiong Mu, Jian Xu, and Shijun Shao

Anal. Chem., **Just Accepted Manuscript** • DOI: 10.1021/acs.analchem.7b04435 • Publication Date (Web): 30 Jul 2018

Chromogenic, Fluorescent and Redox Sensors for Multichannel Imaging and Detection of Hydrogen Peroxide in Living Cell Systems

Yue Ni,[†, ‡] Hong Liu,[†] Di Dai,[†] Xiqiong Mu,[†] Jian Xu[*,†] and Shijun Shao[*,†]

[†] CAS Key Laboratory of Chemistry of Northwestern Plant Resources and Key Laboratory for Natural Medicine of Gansu Province, Lanzhou institute of Chemical Physics, Chinese Academy of Sciences, Lanzhou 730000, P. R. China.

[‡] University of Chinese Academy of Sciences, Beijing 100049, P. R. China.

* Corresponding author: Shijun Shao

Tel: +86-931-4968209

Fax: +86-931-4968019

E-mail: sjshao@licp.cas.cn

ABSTRACT: Hydrogen peroxide (H_2O_2) is an important reactive oxygen species (ROS). Maintaining the H_2O_2 concentration at a normal level is critical to achieve the normal physiological activities of cells, otherwise might trigger various diseases. Therefore, it is necessary to develop new and practical multi-signaling sensors for both visualization of intracellular H_2O_2 and accurate detection of extracellular H_2O_2. In this paper, a novel multichannel signaling fluorescence-electrochemistry combined probe **1** (**FE-H_2O_2**) is presented here for imaging and detection of H_2O_2 in living cell systems. In our design, the probe **FE-H_2O_2** consists of H_2O_2 reaction site and 4-ferrocenyl(vinyl)pyridine unit which affords chromogenic, fluorescent and electrochemical signals. These structural motifs yield a combined chromogenic, fluorescent and redox sensor in a single molecule. Probe **FE-H_2O_2** showed "Turn-On" fluorescence response to H_2O_2, which can be used for monitoring intracellular H_2O_2 in vivo. Furthermore, the electrochemical response of probe **FE-H_2O_2** was decreased after the addition of H_2O_2, which can be applied for accurate detection of H_2O_2 released from living cells. Combined fluorescence imaging method with electrochemical analysis technology, the well-designed multi-module probe is hopeful to serve as a practical tool for the understanding of the metabolism and homeostasis of H_2O_2 in complex biological system.

INTRODUCTION

Hydrogen peroxide (H_2O_2), as an important reactive oxygen species (ROS), plays an essential role in maintaining the physiological balance of organisms in living systems.[1] Aberrant production or accumulation of H_2O_2 would bring about severe damage for proteins and DNA, thus further causing serious human diseases including cancer, diabetes, neurodegenerative Alzheimer's, Parkinson's, and Huntington's diseases.[2-6] Considering the widespread impacts of H_2O_2 homeostasis on human health and disease, it is necessary to develop an effective method for sensitive detection of H_2O_2 level under physiological conditions as well as further visualization of localized production and accumulation of H_2O_2 in living cells.

Up to now, various analytical methods such as photocolorimetry,[7-9] fluorescence,[10-14] chemiluminescence,[15] and electrochemical technologies[16-19] have been employed for H_2O_2 detection. Among them, fluorescence sensing method combined with confocal laser imaging technology has emerged as one of the most powerful and versatile tools for monitoring the localization, and transportation of vital bio-molecules within the context of living systems.[20-21] Although many fluorescent probes have been developed for bioimaging intracellular H_2O_2 dynamics, they still have some limitations for the quantitative detection of the released extracellular H_2O_2 levels due to the relatively low sensitivity.[22-24] To solve this problem, the electrochemical sensor is considered as the most promising candidate due to its high sensitivity, low detection limit, as well as high convenience.[25-31] Recently, based on TiO_2@Cu_2O,[32] Au Nanoparticles-nitrogen-doped graphene quantum dots,[33] PtPb/graphene,[34] and so on,

excellent performance has been achieved in nanocomposite-based electrochemical sensors. These electrochemical analysis platforms can be used for high-sensitivity detection of H_2O_2 released from living cells even with the detection limit as low as nM. Therefore, it is a good idea to combine fluorescence imaging method with electrochemical analysis technology and design the multichannel signaling probes, which can not only realize biological imaging analysis of intracellular H_2O_2 but also fulfill the real-time detection of H_2O_2 released from living cells. Using this multichannel signaling method, we can have more clear understanding of the metabolism and homeostasis of H_2O_2 in the complex biological system. However, to the best of our knowledge, the reported multichannel signaling receptors for H_2O_2 sensing are still rare and thus developing new and practical multi-signaling sensors for both visualization of intracellular H_2O_2 and accurate detection of extracellular H_2O_2 is still a challenge.[35]

Recently, a hemicyanine-based fluorescent probe was developed by our group for monitoring and imaging of mitochondrial H_2O_2 in living cells.[36] Based on the previous work, a novel fluorescence-electrochemistry combined probe **1** (**FE-H_2O_2**) was presented here as a multichannel signaling sensor for imaging and detection of H_2O_2 in living cell systems (**Scheme 1**). In our design, π-conjugate moiety of 4-vinylpyridine salt, widely used to synthesize dyes and fluorescent probes, was utilized as fundamental fluorescence skeleton. Based on the unique oxidative activity of H_2O_2 for boronate,[37] a *p*-pinacolborylbenzyl group was selected as the reaction site for H_2O_2. In addition, a ferrocene unit was introduced here not only as part of the fluorescent conjugate structure but also to afford electrochemical signals. The reaction of **FE-H_2O_2** with H_2O_2

under physiological conditions, which caused the oxidation of the boronate moiety of **FE-H_2O_2** and 1,6-rearrangement elimination reaction, can release **Dye 2**.[36,39] As a result, these structural motifs yield a combined chromogenic, fluorescent and redox sensor in a single molecule. In the chromogenic channel, the addition of H_2O_2 to a buffer solution of **FE-H_2O_2** caused obvious change of color from light-red to colourless, which can be used for a "naked-eye" detection of H_2O_2 effectively. In the fluorescent channel, a "Turn-On" fluorescence response was observed for H_2O_2 determination, which can be applied to monitor intracellular H_2O_2 by cell fluorescence imaging. In the redox channel, the electrochemical response of Fe^{II}/Fe^{III} redox couple was decreased after the addition of H_2O_2, which can be used as a convenient method to detect the trace level of H_2O_2 released from live cells. In light of these desired properties, such as highly selective "Turn-On" fluorescence response, good biocompatibility and low electrochemical detection limit, the multi-signaling probe **FE-H_2O_2** was successfully applied for monitoring and imaging of H_2O_2 in living cells and meanwhile for the accurate detection of H_2O_2 released from living cells.

Scheme 1. Design of Probe **FE-H_2O_2** and Its Reaction with H_2O_2

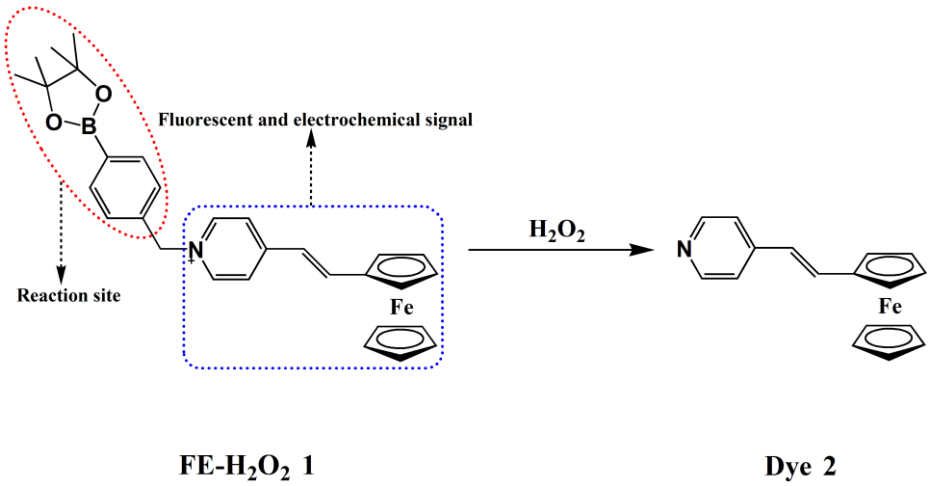

EXPERIMENTAL SECTION

Materials and Apparatus. All reagents were purchased from Sigma-Aldrich and used as received without further purification. All the solvents used were of analytical grade. RAW 264.7 macrophage cells were obtained from the Cell Bank of Type Culture Collection of the Chinese Academy of Sciences (China). Ultrapure water from a Millipore Direct-Q system was used throughout the experiment.

^{1}H NMR and ^{13}C NMR spectra were recorded using a Varian INOVA 400 MHz spectrometer. High-resolution electrospray ionization (ESI) mass spectra were recorded on a Waters micrOTOF-Q II mass spectrometer. Absorption spectra were measured on a PerkinElmer Lambda 35 spectrophotometer. Fluorescence measurements were recorded on a PerkinElmer LS 55 fluorescence spectrophotometer using quartz cuvettes with a path length of 1 cm. Fluorescence images were obtained with confocal laser scanning microscope (Olympus Fluoview FV1200). A Sartorius basic pH-Meter was used for the pH measurements. Cytotoxicity assays were performed in an Epoch ELISA plate reader (BioTek, Winooski, Vermont).

Measurement of Fluorescence Quantum Yield. Fluorescence quantum yield (Φ_{fl}) was determined using fluorescein (Φ_{fl} = 0.90, in 0.1 M NaOH) as standard and calculated according to the following equation:[36]

$$\Phi_{fl}^{sample} = \Phi_{fl}^{standard}\ Abs^{standard}\ \Sigma[F^{sample}] / Abs^{sample}\ \Sigma[F^{standard}]$$

Here, Φ_{fl}^{sample} and $\Phi_{fl}^{standard}$ are the fluorescence quantum yields of the sample and standard, respectively. Abs^{sample} and $Abs^{standard}$ are the respective optical densities of the sample and the reference solution at the wavelength of excitation. $\Sigma[F]$ denotes the

integrated fluorescence intensity.

The synthetic routes for probe **FE-H_2O_2** were shown in **Scheme 2**.

1) Synthesis of Compound 3. Formylferrocene was synthesized according to the reported method.[39] Dimethylformamide (14.6 g, 0.2 mol) was added to a solution of ferrocene (18.6 g, 0.1 mol) in 75 mL of dry chloroform and the resulting mixture was stirred in an ice-bath under nitrogen atmosphere for 10 min. Then, phosphoryl chloride (30.6 g, 0.2 mol) was added dropwise to the mixture. The reaction mixture was kept stirring at 60 °C for 20 h. Chloroform was evaporated and the residue was transferred into water. Solid precipitate was filtered off and the filtrate was extracted repeatedly with ether. The ether extract was washed with water, and the solvent was removed to yield the crude product which was purified by recrystallization from a mixed solvent (dichloromethane/hexane, 3/1, v/v) to afford pure compound **3** (15.2 g, 71%) as reddish-brown crystals. MS (ESI): Calcd for $C_{11}H_{10}FeO$: 214.0081, found: m/z 236.9972 $[M+Na]^+$.

2) Synthesis of Compound 4. A mixture of 4-methylpyridine (1.4 mmol, 0.13 g) and 4-(Bromomethyl)-benzeneboronic acid pinacol ester (1.7 mmol, 0.5 g) in toluene was refluxed at 110 °C for 12 h. The obtained white powdery solid was filtered, washed with toluene and dried in vacuo to afford pure compound **4** (0.27 g, 63%). ^{1}H NMR (CD_3CN, 400 MHz) δ: 8.71 (d, 2H, pyridine-H), 7.86 (d, 2H, pyridine-H), 7.77 (d, 2H, Ar-H), 7.46 (d, 2H, Ar-H), 5.73 (s, 2H, CH_2), 2.61 (s, 3H, CH_3), 1.31(s, 12H, CH_3). ^{13}C NMR (CD_3CN, 400 MHz): δ 21.8, 24.7, 63.9, 75.2, 84.9, 128.4, 128.8, 129.5, 135.4,

135.9, 136.9, 144.2. MS (ESI): Calcd for $[C_{19}H_{25}BNO_2]^+$: 310.1982, found: m/z 310.1808 $[M]^+$.

3) Synthesis of Probe FE-H_2O_2 (1). Compound **3** (1 mmol, 0.21 g) and compound **4** (1 mmol, 0.31 g) were mixed in ethanol (20 mL), and then piperidine (0.05 mL) was added to the solution. The reaction mixture was refluxed with stirring for 1 h and then evaporated in vacuo. The resulting solid was dissolved in CH_2Cl_2, and the organic layer was washed three times with water, dried over anhydrous $MgSO_4$, and evaporated in vacuo. The crude product was purified by silica gel column chromatography using CH_2Cl_2/MeOH (10/1, v/v) as the eluent, resulting in **FE-H_2O_2 (1)** (0.13 g, 26%) as a purple solid. ^{1}H NMR (CD_3CN, 400 MHz): 8.53-8.56 (m, 4H, pyridine-H), 7.85-7.89 (m, 5H, ferrocene-H), 7.77-7.81 (m, 4H, ferrocene-H), 7.41-7.45 (m, 4H, Ar-H), 6.86 (d, 2H, vinylic), 5.60 (s, 2H, benzyl-CH_2), 1.31 (s, 12H, CH_3). ^{13}C NMR (CD_3CN, 400 MHz): δ 24.0, 48.9, 69.3, 72.3, 74.6, 119.4, 123.0, 128.1, 135.4, 143.6, 144.8, 154.3. MS (ESI): Calcd for $[C_{30}H_{33}BFeNO_2]^+$: 506.1959, found: m/z 506.1952 $[M]^+$.

Scheme 2. Synthesis of Probe FE-H_2O_2 (1)

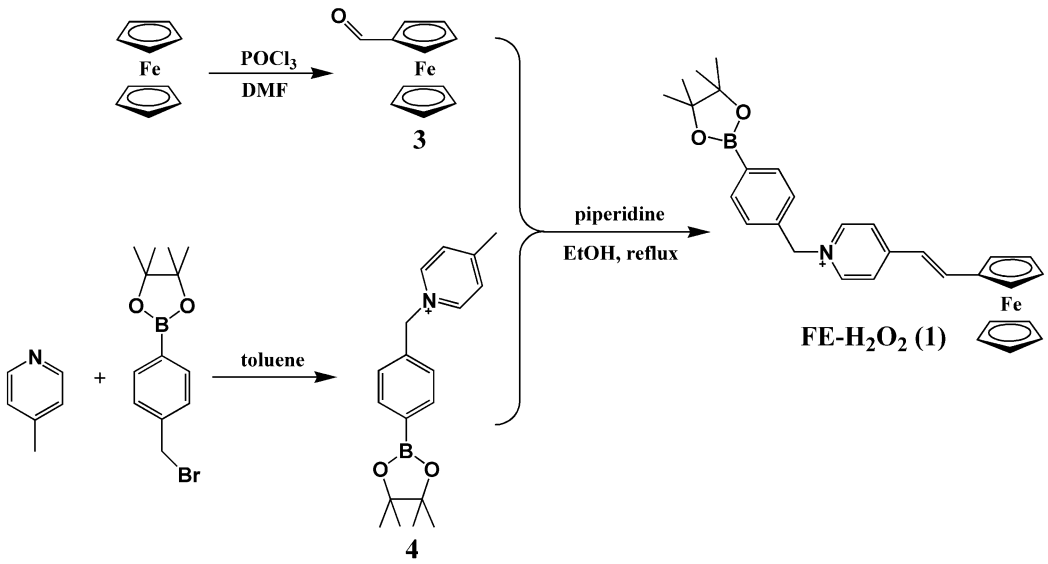

Electrochemical Measurements. Electrochemical experiments were conducted on a CHI660C electrochemical workstation (CH Instruments, Shanghai Chenhua Instrument Corporation, China) in a conventional three-electrode configuration. A bare glass carbon electrode (GCE), a platinum wire and a Ag/AgCl (3 M KCl) electrode were used as the working electrode, auxiliary electrode and reference electrode, respectively. Before the measurement, the bare GCE (3 mm) was carefully polished with 1.0, 0.3 and 0.05 μm alumina slurry, and cleaned by ultrasonic treatment in 50% nitric acid, water and acetone for 5 min, respectively. 20 mM phosphate buffer solution (PBS, pH 7.4) was used as the supporting electrolyte and deoxygenated by bubbling with high-pure nitrogen for 30 min before electrochemical experiments. The cyclic voltammetric and differential pulse voltammetric measurements were performed in a potential range of 0-1.0 V and the current was recorded after the addition of different concentrations of H_2O_2 into 5 mL of CH_3CN/PBS (1:9 v/v) containing 0.1 mM **FE-H_2O_2**.

Computational study. Geometry optimizations for gas-phase molecules were performed with the Gaussian 09 software package by using density functional theory (DFT) calculations. The adopted exchange-correlation functional was B3LYP with Becke's three parameter form,[40,41] in which the nonlocal correlation was expressed by Lee-Yang-Parr functional,[42] and the local correlation part was by the Vosko-Wilk-Nusair III functional.[43] The basis set of 6-311+G** was used in DFT calculations.

Detection of H_2O_2 Released from Cells. The RAW 264.7 macrophage cells were grown to 90% confluence at 37 °C in 5% CO_2 in 75 cm^2 flasks and the number of cells was about 3×10^6. Then the cells were washed by PBS (pH 7.4) for three times and

dispersed into 2 mL PBS accompanied by 1 μM PMA injection. After cultivation for different time (0 min, 30 min, 45 min, 60 min, 75 min and 90 min), the supernant was sucked out and added to 0.1 mM **FE-H_2O_2** for differential pulse voltammetry (DPV) experiments in a potential range of 0-1.0 V and the recorded peak current was obtained. Then, the concentration of H_2O_2 released from cells was calculated by the obtained calibration equations.

Cytotoxicity Assays. The cell viability was measured by CCK-8 assay technique. The RAW 264.7 macrophage cells were seeded in 96 well plates and incubated in 200 μL fresh medium with or without various concentrations of **FE-H_2O_2** for 24 h. Then, the medium was removed and replaced with 100 μL fresh medium adding 10 μL CCK-8 assay agents for 4 h. Subsequently, the fluorescence intensity of the solution with 450 nm excitation was measured in an ELISA Epoch plate reader. Four separate measurement results were analyzed using Gen5 data analysis software (BioTek).

RESULTS AND DISCUSSION

Chromogenic and Fluorescent Response of Probe FE-H_2O_2 to H_2O_2. The determination of H_2O_2 with probe **FE-H_2O_2** was investigated in CH_3CN/PBS (1:99 v/v, 20 mM, pH 7.4) at room temperature (25°C). Probe **FE-H_2O_2** displayed two major absorption band centered at 360 nm and 540 nm respectively. When H_2O_2 was added to the solution of probe **FE-H_2O_2**, the absorption band of 360 nm was slightly red-shifted and the long-wave absorption at 540 nm was almost disappeared, due to the H_2O_2-induced oxidation of probe **FE-H_2O_2** to release **Dye 2**. Meanwhile, a prominent

color change from light-red to colourless was observed (Figure 1A), which suggested H_2O_2 can be detected with "naked-eye" in the chromogenic channel.

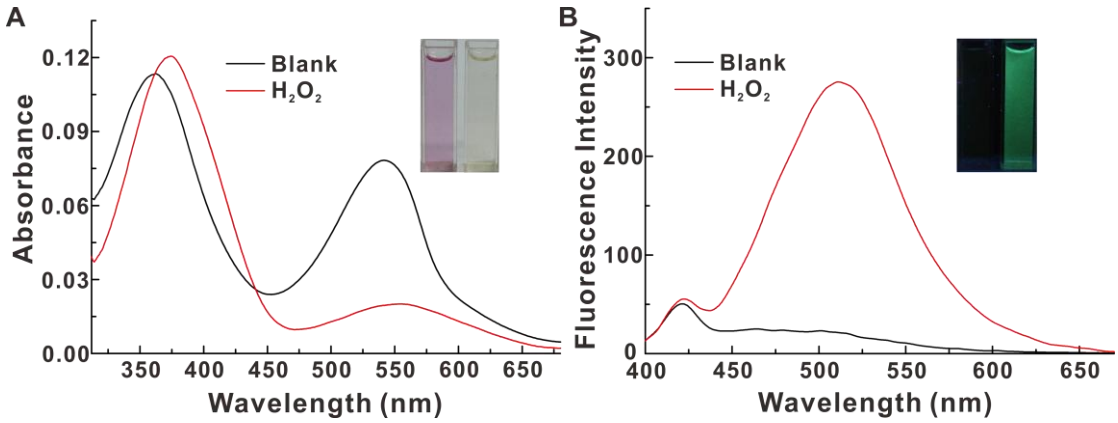

Figure 1. Absorption (A) and fluorescence (B) spectra of probe **FE-H_2O_2** (10 μM, black line), and the reaction mixture (red line) of 10 μM probe **FE-H_2O_2** with 50 μM H_2O_2 in CH_3CN/PBS (1:99 v/v, 20 mM, pH 7.4), λ_{ex} = 360 nm with slit: 10 nm, 10 nm. The inset shows the color change (A) and fluorescence change (B) of probe **FE-H_2O_2** in the absence and presence of H_2O_2 under visible light or UV light at 365 nm.

In the fluorescent channel, probe **FE-H_2O_2** (Φ_{fl} = 0.0034) featured a negligible emission at 512 nm. However, a dramatic increase of fluorescence intensity at 512 nm (13-fold fluorescence increase) was triggered upon addition of H_2O_2 to the solution of **FE-H_2O_2**, accompanied by the emergence of an obvious green-colored fluorescence (Figure 1B and Figure S7). The results indicated that probe **FE-H_2O_2** displayed a good sensitivity for H_2O_2 detection in abiotic systems.[23,44] In addition, the emission titration experiments of probe **FE-H_2O_2** (10 μM) with H_2O_2 at varied concentrations were performed. The fluorescence intensity of the system was enhanced with the increase of H_2O_2 concentration, and there was a good linearity between the emission intensity at 512 nm and the H_2O_2 concentrations in the range from 2.0 to 50 μM (Figure S8).

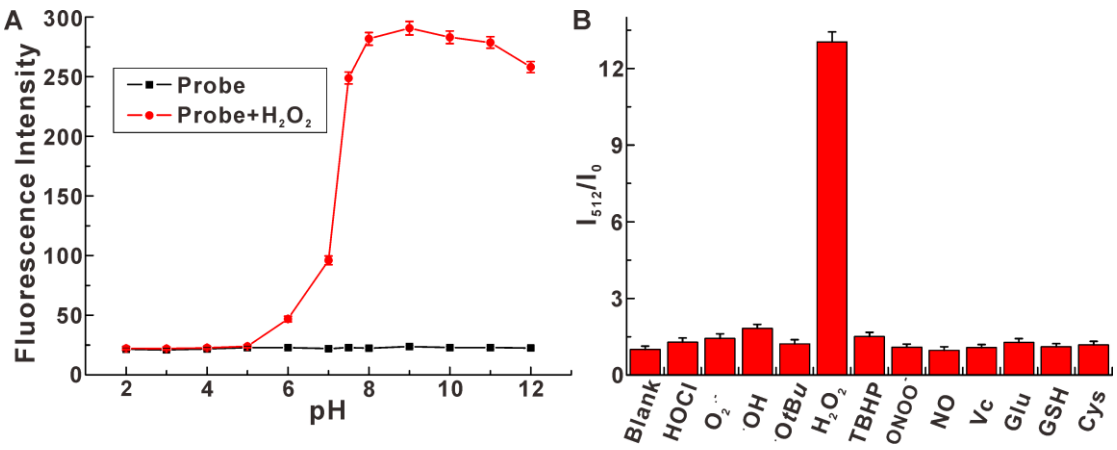

Figure 2. (A) Fluorescence intensity of 10 μM probe **FE-H_2O_2** with the addition of 50 μM H_2O_2 at various pH values. (B) Fluorescence responses of 10 μM probe **FE-H_2O_2** to 50 μM various reactive oxygen species (ROS), reactive nitrogen species (RNS), ascorbic acid, glucose, GSH and cysteine. The error bars represent standard deviation of three measurements.

Effects of pH and Selectivity Studies. The pH-dependence of probe **FE-H_2O_2** was next investigated in the detection of H_2O_2. As shown in Figure 2A, the fluorescence intensity dramatically increased when the pH value was higher than 5.0 and reached a peak value about 9.0. It is mainly because arylboronic acids can only react with H_2O_2 under mild alkaline conditions to generate phenols and the phenomenon has been demonstrated by other groups.[38,45] Besides, the fluorescent emission of the probe alone was changeless at various pH, which convinced the stability of probe **FE-H_2O_2**.

The potential interfering effect of various reactive oxygen species (ROS) and reactive nitrogen species (RNS) on the reaction of probe **FE-H_2O_2** with H_2O_2 was also evaluated. As shown in Figure 2B, only H_2O_2 induced a dramatic fluorescence enhancement, while other ROS (HOCl, $O_2^{\bullet-}$, •OH, •O*t*Bu, TBHP), RNS ($ONOO^-$, NO), ascorbic acid, glucose, GSH and cysteine triggered no or very minor changes. The excellent selectivity was ascribed to the H_2O_2-specific boronate deprotection reaction and the ambiphilic properties of H_2O_2.[1]

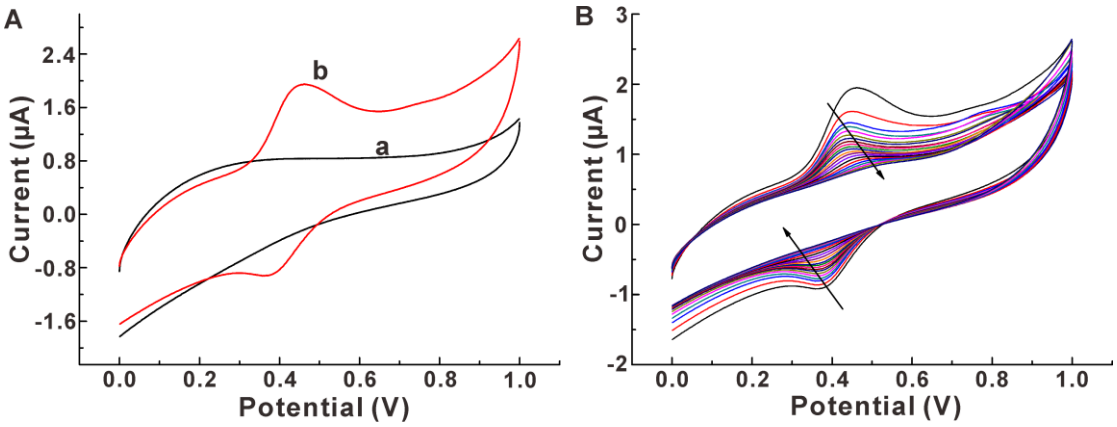

Figure 3. (A) CVs of bare GCE in N_2-saturated 20 mM PBS in the absence (a) and presence (b) of 100 μM **FE-H_2O_2** at a scan rate of 100 mVs^{-1}. (B) CVs of bare GCE in N_2-saturated CH_3CN/PBS (1:9 v/v) containing 100 μM **FE-H_2O_2** in the presence of different concentrations of H_2O_2 (0, 0.1, 0.2, 0.3, 0.4, 0.5, 1, 1.5, 2, 2.5, 3, 4, 5, 6, 7, 8, 13, 18, 23, 28 and 33 μM) at a scan rate of 100 mV/s.

Electrochemical Detection of H_2O_2. In the redox channel, cyclic voltammetry was firstly used to investigate the recognition ability of **FE-H_2O_2** towards H_2O_2. Compared with the cyclic voltammogram (CV) of bare GCE in N_2-saturated 20 mM PBS, a pair of redox peaks attributed to one-electron redox process of **FE-H_2O_2** were observed when 100 μM **FE-H_2O_2** was injected. The anodic and cathodic peak potential of **FE-H_2O_2** was around 0.46 V and 0.38 V, respectively (Figure 3A). When H_2O_2 was added to the solution of **FE-H_2O_2**, both the anodic and cathodic peak currents decreased with the increase of the concentrations of H_2O_2 with slight peak potential shifts (Figure 3B). The obvious changes of CVs were ascribed to the oxidation reaction of **FE-H_2O_2** with H_2O_2 and the release of **Dye 2**.

We next used differential pulse voltammetry to investigate the reaction between **FE-H_2O_2** and H_2O_2. Differential pulse voltammograms (DPVs) of bare GCE with successive addition of different concentrations of H_2O_2 were recorded in 5 mL of

CH_3CN/PBS (1:9 v/v) containing 100 μM **FE-H_2O_2**. As observed in Figure 4A, the peak current gradually decreased with the addition of H_2O_2, which was similar to the result of CV experiments. Exponential fitting curve of the peak current to H_2O_2 concentration was obtained in the range of 0 to 83 μM (Figure 4B). The detection limit toward H_2O_2 using **FE-H_2O_2** probe was determined to be 0.1 μM, which was lower than most reported fluorescence methods for H_2O_2 detection.[46-49]

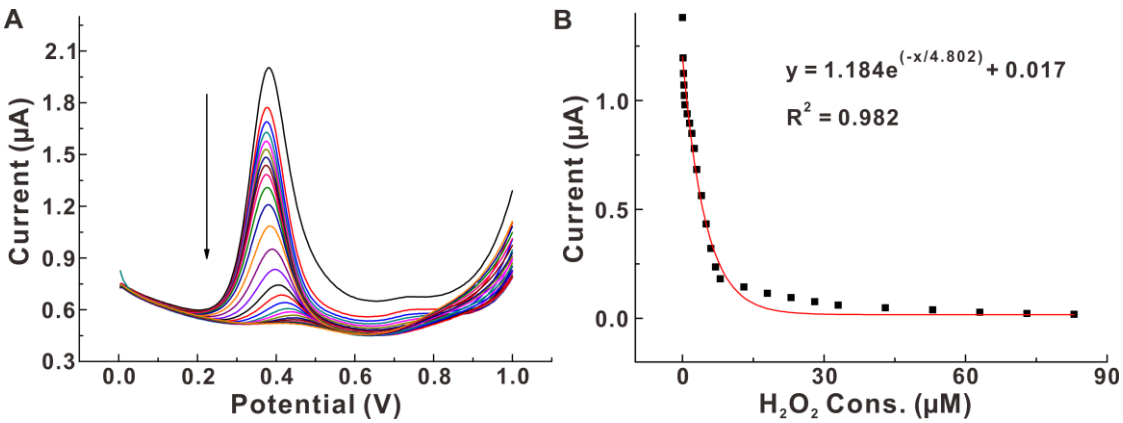

Figure 4. (A) DPVs of bare GCE in N_2-saturated CH_3CN/PBS (1:9 v/v) containing 100 μM **FE-H_2O_2** in the absence and presence of different concentrations of H_2O_2 from 0 to 83 μM. (B) The exponential fitting curve between the peak current and the concentration of H_2O_2.

Mechanism Studies and Density Functional Theory (DFT) Calculation. The high resolution mass spectroscopy analysis of the reaction solution of **FE-H_2O_2** with H_2O_2 was conducted to confirm the reaction mechanism (Figure S19), and the observed peak at m/z 290.0651 $[M+H]^+$ was reasonably assigned to **Dye 2**. Furthermore, 4-ferrocenyl(vinyl)pyridine (**Dye 2**) was synthesized and characterized by ^{1}H NMR and ESI-MS analysis (Figure S17 and Figure S18). The absorption spectra, fluorescence spectra, CV and DPV of **Dye 2** were also detected (Figure S1-S4). The comparison of the experimental results between the pure **Dye 2** and the reaction product of **FE-H_2O_2**

with H_2O_2 showed that the proposed reaction mechanism is valid (**Scheme 1**).

Molecular geometry optimizations were performed with the Gaussian 09 software package by using density functional theory (DFT) methods with B3LYP hybrid exchange–correlation functional and the B3LYP/6-311+G** basis set. As shown in Figure 5, the LUMO energy level of 4-(pinacolboryl)benzyl pyridine cation moiety (-6.33 eV) of probe **FE-H_2O_2** was much lower than that of ferrocene unit (-0.37 eV), and thus probe **FE-H_2O_2** (Φ_{fl} = 0.0034) displayed quenched fluorescence due to the PET process. As for the reaction product Dye 2, the LUMO energy level of the pyridine moiety (-1.13 eV) was comparable to that of ferrocene unit (-0.37 eV). Therefore, the PET process was prohibited, and product Dye **2** (Φ_{fl} = 0.17) should be fluorescent.

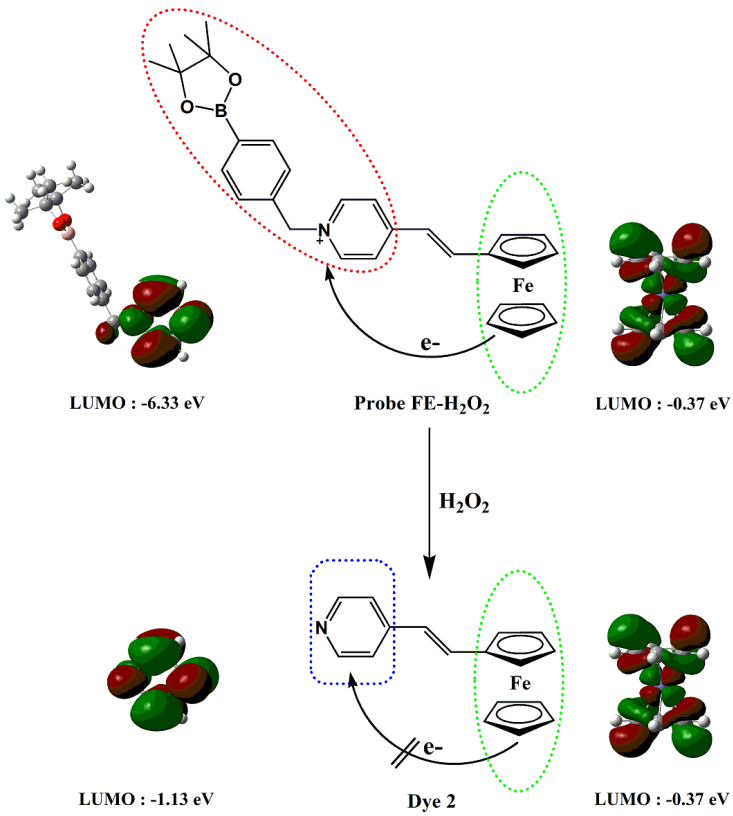

Figure 5. LUMO energy level comparison of probe **FE-H_2O_2** and Dye **2**.

Real-time imaging intracellular H_2O_2 and detection of H_2O_2 released from cells. As an important signal molecule, H_2O_2 can penetrate through cell membrane and the intracellular or extracellular H_2O_2 concentration is in a dynamic balance.[50] Under endogenous or exogenous stimuli, the physiological H_2O_2 concentration is everchanging due to its continuous generation and degradation, resulting in different physiological and pathological consequences.[51] In this regard, probe **FE-H_2O_2** can be effectively used for both imaging intracellular H_2O_2 and the detection of H_2O_2 released from cells.

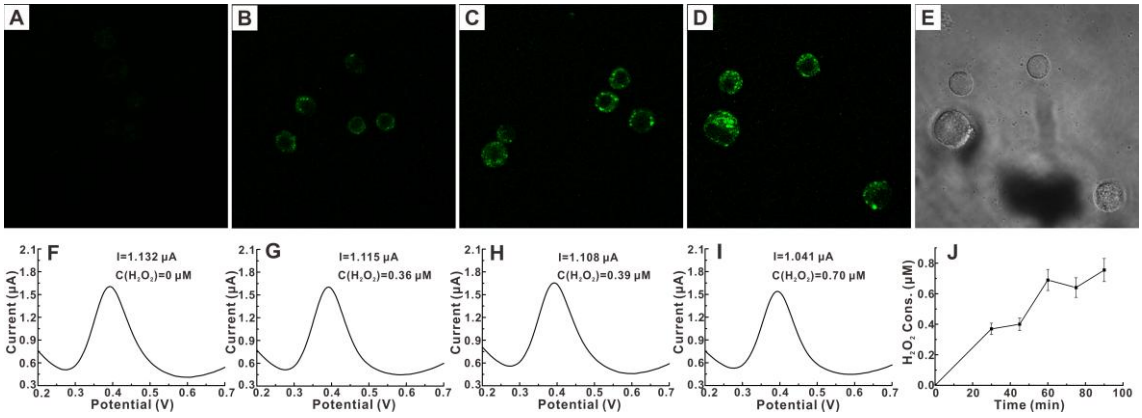

Figure 6. Confocal fluorescence images of RAW 264.7 cells incubated with 10 μM probe **FE-H_2O_2** for 30 min at 37 °C. Probe-stained macrophage cells stimulated with 1 μg/mL PMA for different time: (A) 0 min, (B) 30 min, (C) 45 min, (D) 60 min, (E) Bright field of (D). The corresponding DPVs of bare GCE in N_2-saturated cells culture solution containing 100 μM **FE-H_2O_2** with different stimulation time: (F) 0 min, (G) 30 min, (H) 45 min, (I) 60 min (the value of "I" was the peak current after the deduction of baseline). (J) The change of H_2O_2 released from macrophage cells with the increasing of stimulation time.

We firstly examined the feasibility of probe **FE-H_2O_2** to detect endogenous produced H_2O_2 in living macrophage cells. When stimulated by phorbol myristate acetate (PMA), macrophage cells could produce endogenous H_2O_2.[21,23] The living RAW 264.7 macrophage cells loaded with only the probe **FE-H_2O_2** (10 μM) displayed almost no fluorescence (Figure 6A). However, when the pretreated macrophage cells were

incubated with 1 μg/mL PMA for 30 min, obvious bright-green fluorescence was observed. Furthermore, the fluorescence intensity was enhanced with the time increasing from 30 min to 60 min (Figure 6B-6D). These results demonstrated that with the increase of incubation time of cells with PMA, the intracellular H_2O_2 was produced and accumulated. The probe **FE-H_2O_2** was capable of visualization the H_2O_2 burst at natural immune response levels.

In order to figure out the H_2O_2 metabolism in the PMA-induced immune process, **FE-H_2O_2** was simultaneously utilized to detect H_2O_2 released from RAW 264.7 cells with electrochemical method. In the DPVs, the peak current decreased with the increase of incubation time of cells with 1 μg/mL PMA. The phenomenon indicated that different concentrations of H_2O_2 were released from macrophage cells upon stimulation. As observed in Figure 6G-6I, the concentration of H_2O_2 released increased with the time and reached a peak at 60 min. And then, the concentration of H_2O_2 increased slowly and maintained stable after 60 min (Figure 6J and Figure S9). In contrast, no current change was observed without stimulation, indicating that there was no H_2O_2 released from the RAW 264.7 cells (Figure 6F). Notablely, the changes of H_2O_2 released from macrophage cells were approximately consistent with the fluorescence changes within the cells, which revealed the dynamic changes of H_2O_2 in the immune process. Moreover, the cytotoxicity assay was performed to evaluate the biocompatibility of the probe **FE-H_2O_2** (Figure S10). As the concentration of **FE-H_2O_2** increased from 0.5 to 10 μM, no significant toxicities were showed, which meant the potential application of **FE-H_2O_2** in live cell systems.

CONCLUSIONS

In summary, a new multi-module probe **FE-H_2O_2** has been designed and constructed here for imaging and detection of H_2O_2 in living cell systems. In the optical channel, obvious color change from light-red to colourless was observed upon addition of H_2O_2 to the buffer solution of **FE-H_2O_2**, which makes it possible for "naked-eye" detection of H_2O_2. In the fluorescent channel, probe **FE-H_2O_2** displayed highly sensitive and selective "Turn-On" fluorescence response to H_2O_2, which can be applied to monitor intracellular H_2O_2 activity using fluorescence sensing method with confocal laser imaging technology. In the redox channel, the electrochemical response of probe **FE-H_2O_2** was decreased after the addition of H_2O_2, which can be utilized as a convenient method to detect the trace level of H_2O_2 released from live cells. Therefore, this multi-module multichannel probe is hopeful to serve as a practical tool for deeply understanding of the metabolism and homeostasis of H_2O_2 in complex biological system and inspire the production of new specific fluorescence-electrochemistry combined sensor devices.

ASSOCIATED CONTENT

Supporting Information

Additional information includes preparation of various ROS and RNS, synthesis and characterization of dye **2**, time course, chromogenic titration and fluorescence titration of probe **FE-H_2O_2** to H_2O_2, DPV detection of H_2O_2 released from cells, cell culture and imaging, cytotoxicity assay, nucleated staining, ^{1}H NMR, ^{13}C NMR and MS spectra.

ACKNOWLEDGMENTS

The authors acknowledge the financial support for this work by the National Natural Science Foundation of China (21572239 and 21505145), the Personnel Training Project of the West Light Foundation of the Chinese Academy of Sciences (2016, to Jian Xu) and the top priority program of "One-Three-Five" Strategic Planning of Lanzhou Institute of Chemical Physics, CAS. We acknowledge National Supercomputing Center in Shenzhen for providing the computational resources and the Gaussian 09 package. We gratefully thank Dr. Yan Zhang (Northwest Normal University, China) for the help of computational study and Dr. Feifei Li (Institute of Modern Physics, CAS) for the help of cytotoxicity assay.

REFERENCES

(1) Lippert, A. R.; Van de Bittner, G. C.; Chang, C. J. *Acc. Chem. Res.* **2011**, *44*, 793-804.

(2) William, R. M. *Free Radical Bio. Med.* **1997**, *23*, 134-147.

(3) Guy, M. C.; Daniel, S. *Free Radical Bio. Med.* **2000**, *28*, 1815-1826.

(4) Alex, S.; Fulvio, U. *Free Radical Bio. Med.* **2000**, *29*, 306-311.

(5) Ohshima, H.; Tatemichi, M.; Sawa, T. *Arch. Biochem. Biophys.* **2003**, *417*, 3-11.

(6) Shah, A. M. *Heart.* **2004**, *90*, 486-487.

(7) Chen, S.; Hai, X.; Chen, X. W.; Wang, J. H. *Anal. Chem.* **2014**, *86*, 6689-6694.

(8) Nasir, M.; Rauf, S.; Muhammad, N.; Hasnain Nawaz, M.; Anwar Chaudhry, A.; Hamza Malik, M.; Ahmad Shahid, S.; Hayat, A. *J. Colloid Interf. Sci.* **2017**, *505*, 1147-1157.

(9) Zhang, L.; Hai, X.; Xia, C.; Chen, X. W.; Wang, J. H. *Sensor. Actuat. B: Chem.* **2017**, *248*, 374-384.

(10) Maeda, H.; Fukuyasu, Y.; Yoshida, S.; Fukuda, M.; Saeki, K.; Matsuno, H.; Yamauchi, Y.; Yoshida,

K.; Hirata, K.; Miyamoto, K. *Angew. Chem. Int. Edit.* **2004**, *43*, 2389-2391.

(11) Maki, O.; Seiichi, U.; Atsushi, E.; Hidetoshi, T.; Tomofumi, S.; Kazuhiro, I. *Org. Lett.* **2003**, *5*, 1459-1461.

(12) Miller, E. W.; Albers, A. E.; Pralle, A.; Isacoff, E. Y.; Chang, C. J. *J. Am. Chem. Soc.* **2005**, *127*, 16652-16659.

(13) Xu, K.; Tang, B.; Huang, H.; Yang, G.; Chen, Z.; Li, P.; An, L. *Chem. Commun.* **2005**, 5974-5976.

(14) Albers, A. E.; Okreglak, V. S.; Chang, C. J. *J. Am. Chem. Soc.* **2006**, *128*, 9640-9641.

(15) Chen, W.; Cai, S.; Ren, Q. Q.; Wen, W.; Zhao, Y. D. *Analyst.* **2012**, *137*, 49-58.

(16) Karsten, A. F.; Miloslav, P.; George G. G. *Talanta*. **2001**, *54*, 531-559.

(17) Muench, F.; Felix, E.-M.; Rauber, M.; Schaefer, S.; Antoni, M.; Kunz, U.; Kleebe, H.-J.; Trautmann, C.; Ensinger, W. *Electrochim. Acta*. **2016**, *202*, 47-54.

(18) Lou, X.; Zhu, C.; Pan, H.; Ma, J.; Zhu, S.; Zhang, D.; Jiang, X. *Electrochim. Acta*. **2016**, *205*, 70-76.

(19) Behera, T. K.; Sahu, S. C.; Satpati, B.; Bag, B.; Sanjay, K.; Jena, B. K. *Electrochim. Acta*. **2016**, *206*, 238-245.

(20) Daims, H.; Nielsen, J. L.; Nielsen, P. H.; Schleifer, K. H.; Wagner, M. *Appl. Environ. Microb.* **2001**, *67*, 5273-5284.

(21) Srikun, D.; Miller, E. W.; Domaille, D. W.; Chang, C. J. *J. Am. Chem. Soc.* **2008**, *130*, 4596-4597.

(22) Bryan, C. D.; Calvin, H.; Christopher, J. C. *J. Am. Chem. Soc.* **2010**, *132*, 5906–5915.

(23) Abo, M.; Urano, Y.; Hanaoka, K.; Terai, T.; Komatsu, T.; Nagano, T. *J. Am. Chem. Soc.* **2011**, *133*, 10629-10637.

(24) Hitomi, Y.; Takeyasu, T.; Funabiki, T.; Kodera, M. *Anal. Chem.* **2011**, *83*, 9213-9216.

(25) Han, Y.; Zheng, J.; Dong, S. *Electrochim. Acta*. **2013**, *90*, 35-43.

(26) Ke, X.; Li, Z.; Gan, L.; Zhao, J.; Cui, G.; Kellogg, W.; Matera, D.; Higgins, D.; Wu, G. *Electrochim. Acta.* **2015**, *170*, 337-342.

(27) Kulagina, N. V.; Michael, A. C. *Anal. Chem.* **2003**, *75*, 4875-4881.

(28) Inoue, K. Y.; Ino, K.; Shiku, H.; Kasai, S.; Yasukawa, T.; Mizutani, F.; Matsue, T. *Biosens. Bioelectron.* **2010**, *25*, 1723-1728.

(29) Gonzalez-Sanchez, M. I.; Gonzalez-Macia, L.; Perez-Prior, M. T.; Valero, E.; Hancock, J.; Killard, A. J. *Plant. Cell. Environ*. **2013**, *36*, 869-878.

(30) Zhao, J.; Yan, Y.; Zhu, L.; Li, X.; Li, G. *Biosens. Bioelectron.* **2013**, *41*, 815-819.

(31) Reid, C. H.; Finnerty, N. J. *Sensors*. **2017**, *17*, 1596.

(32) Li, Z.; Xin, Y.; Zhang, Z. *Anal. Chem.* **2015**, *87*, 10491-10497.

(33) Ju, J.; Chen, W. *Anal. Chem.* **2015**, *87*, 1903-1910.

(34) Sun, Y.; Luo, M.; Meng, X.; Xiang, J.; Wang, L.; Ren, Q.; Guo, S. *Anal. Chem.* **2017**, *89*, 3761-3767.

(35) Zhang, P.; Zhao, X.; Ji, Y.; Ouyang, Z.; Wen, X.; Li, J.; Su, Z.; Wei, G. *J. Mater. Chem. B.* **2015**, *3*, 2487-2496.

(36) Xu, J.; Zhang, Y.; Yu, H.; Gao, X.; Shao, S. *Anal. Chem.* **2016**, *88*, 1455-1461.

(37) Lo, L. C.; Chu, C. Y. *Chem. Commun.* **2003**, 2728.

(38) Ren, M.; Deng, B.; Zhou, K.; Kong, X.; Wang, J. Y.; Lin, W. *Anal. Chem.* **2017**, *89*, 552-555.

(39) Masaru, S.; Hiromichi, K.; Mikio, S.; Izumi, M.; Kazuo, H. *B. Chem. Soc. Jpn.* **1968**, *41*, 252.

(40) Becke, A. D. *J. Chem. Phys.* **1993,** *98*, 5648-5652.

(41) Stephens, P.; Devlin, F.; Chabalowski, C.; Frisch, M. J. *J. Phys. Chem.* **1994,** *98*, 11623-11627.

(42) Lee, C.; Yang, W.; Parr, R. G. *Phys. Rev. B.* **1988,** *37*, 785-789.

(43) Vosko, S.; Wilk, L.; Nusair, M. *Can. J. Phys.* **1980,** *58*, 1200-1211.

(44) Yuan, L.; Lin, W.; Xie, Y.; Chen, B.; Zhu, S. *J. Am. Chem. Soc.* 2012, *134*, 1305-1315.

(45) Karton-Lifshin, N.; Segal, E.; Omer, L.; Portnoy, M.; Satchi-Fainaro, R.; Shabat, D. *J. Am. Chem. Soc.* **2011**, *133*, 10960-10965.

(46) Ma, Q.; li, X.; Zhang, J.; Zhu, X.; Zhou, L.; Liu, H. *Anal. Methods.* **2017**, *9*, 4558-4565.

(47) Peng, J.; Hou, X.; Zeng, F.; Wu, S. *Biosens. Bioelectron.* **2017**, *94*, 278-285.

(48) Yang, H.; Li, F.; Zou, C.; Huang, Q.; Chen, D. *Microchim. Acta.* **2017**, *184*, 2055-2062.

(49) Huan, Y. F.; Fei, Q.; Shan, H. Y.; Wang, B. J.; Xu, H.; Feng, G. D. *Analyst.* **2015**, *140*, 1655-1661.

(50) Martin-Ventura, J. L.; Madrigal-Matute, J.; Martinez-Pinna, R.; Ramos-Mozo, P.; Blanco-Colio, L. M.; Moreno, J. A.; Tarin, C.; Burillo, E.; Fernandez-Garcia, C. E.; Egido, J.; Meilhac, O.; Michel, J. B. *Thromb. Haemostasis.* **2012**, *108*, 435-442.

(51) Veal, E. A.; Day, A. M.; Morgan, B. A. *Mol. Cell.* **2007**, *26*, 1-14.

Table of Contents Graphic